A Cooling Strategy to Suppress Thermal Runaway in Lithium-Ion Battery Systems

Patcharin Saechan[1*], and *Isares* Dhuchakallaya[2†]

[1]Department of Mechanical and Aerospace Engineering, Faculty of Engineering, King Mongkut's University of Technology North Bangkok, Bangsue, Bangkok, 10800, THAILAND
[2]Faculty of Engineering, Thammasat School of Engineering, Thammasat University, Klong-Luang, Pathumthani, 12120 THAILAND

Abstract. Lithium-ion batteries are essential for electric vehicles and energy storage systems owing to their high energy density and long cycle life. Nonetheless, thermal runaway (TR) remains a critical safety challenge: excessive heat from abuse conditions can trigger exothermic reactions that propagate across cells, leading to catastrophic module failure. This study presents a three-dimensional thermal model of a pressurized air cooling system designed to enhance heat dissipation and suppress runaway propagation in large-scale battery packs. A Tesla Model S module is used for model validation. The influence of airflow conditions and initial failure locations on propagation behavior is systematically investigated. Results show that higher Reynolds numbers (Re) reduce the temperatures of cells adjacent to the failure site, effectively slowing propagation, while sidewall failures generate higher temperatures due to additional radiative heat. Under normal operation, pressurized cooling with Re above 21,000, corresponding to a heat transfer coefficient of 65 $W/m^2 \cdot K$, maintains both peak temperature and temperature uniformity within safe operating limits. TR propagation across the module is fully suppressed when Re exceeds 48,000. These findings highlight the effectiveness of pressurized air cooling in mitigating TR risks in large battery modules.

1 Introduction

The rapid growth of electric vehicles (EVs), renewable energy systems, and portable electronics has placed Lithium-ion batteries (LIBs) at the core of modern energy storage technologies. With their high energy density, long cycle life, and superior charge–discharge efficiency, LIBs have become the dominant choice. Ongoing advancements have further enhanced their performance, enabling higher energy densities and faster charging rates, thereby consolidating their role as the leading solution for future energy systems.

The onset of TR depends strongly on cell chemistry. Cathode materials such as LCO, NCA, and NMC exhibit relatively low onset temperatures (150–200 °C), making them more susceptible to TR, while LFP offers superior thermal stability, often exceeding 230 °C [1, 2].

* Corresponding author: patcharin.s@eng.kmutnb.ac.th
† Corresponding author: disares@engr.tu.ac.th

Additional triggers include decomposition of the electrolyte (60–130 °C), breakdown of the solid electrolyte interphase (~80 °C), and separator melting (130–160 °C), each of which accelerates heat generation and gas release. The accumulation of heat and flammable gases increases internal pressure, ultimately causing venting or rupture, after which flames and radiative heat rapidly ignite adjacent cells.

As such, battery thermal management systems (BTMSs) remain crucial to preventing initiation and suppressing propagation. Effective BTMSs must maintain cell temperatures below 40 °C and minimize non-uniformity (<5 °C) [3]. Liquid cooling offers high heat dissipation capacity but adds weight and complexity, while air cooling is lightweight, cost-effective, and commonly adopted in small-to-medium EVs [4]. However, conventional air cooling is inadequate under severe thermal abuse, motivating research into enhanced convective solutions [5].

Recent studies [6, 7] demonstrate that raising the convective heat transfer coefficient above 40–70 W/m²·K can significantly delay or even suppress TRP. Moreover, cell arrangement and module geometry influence propagation severity, with aligned configurations and increased cell spacing shown to reduce cascading failures. Nevertheless, most prior work has focused on single-cell behavior, leaving uncertainties regarding TR dynamics in large-scale modules. In particular, the role of high-pressure airflow in suppressing runaway has been insufficiently studied.

This research addresses these gaps by developing a three-dimensional thermal model of a pressurized air cooling system to investigate TRP in a large-format battery module. Using a Tesla Model S pack as a case study, the model explores the effects of airflow conditions and failure locations on propagation dynamics, providing new insights into the effectiveness of pressurized cooling as a mitigation strategy.

2 Model description

A representative battery module from the Tesla Model S contains 444 cylindrical Panasonic NCR18650B cells, arranged in a 74P6S configuration. The inter-cell spacing was fixed at 1 mm to reflect realistic space optimization in commercial designs. Six potential failure initiation sites were considered: FB1, FB2, FB3, FB4, FB5, and FB6, as illustrated in Fig. 1. These failure locations were chosen to capture variations in thermal behavior due to both geometry and airflow distribution within the module. In each case, TR was triggered in the designated cell by applying a constant 20C-rate over-discharge.

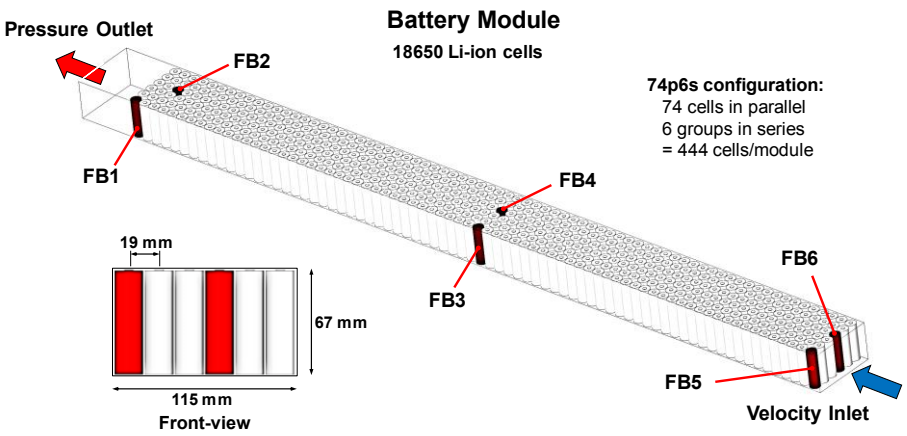

Fig. 1. Schematic of the battery module and the failure positions.

The NCR18650B cell consists of a graphite anode, $LiNi_{0.8}Co_{0.15}Al_{0.05}O_2$ (NCA) cathode, and $LiPF_6$ electrolyte in an EC–DMC–DEC solvent system. The cell has a nominal capacity of 3250–3350 mAh, and a nominal voltage of 3.6 V. The anisotropic thermal conductivity is particularly important: radial conductivity (0.95 W/m·K) is far lower than axial and tangential conductivities (37.1 W/m·K). The density and specific heat capacity were taken as 3602 kg/m³ and 777 J/kg·K, respectively [8].

Three-dimensional thermal-fluid model was developed in ANSYS Fluent to simulate the coupled heat transfer and fluid flow during TRP under pressurized air cooling. Besides conductive heat within the LIB, convective and radiative heat transferred from the battery surfaces are definitely necessary in the propagation behavior of thermal abuse. The fluid flow and the heat transfer are governed by these equations:

$$\frac{\partial \rho_f}{\partial t} + \nabla \cdot (\rho_f \vec{v}_f) = 0 \tag{1}$$

$$\frac{\partial (\rho_f \vec{v}_f)}{\partial t} + \nabla \cdot (\rho_f \vec{v}_f \vec{v}_f) = -\nabla p + \frac{\mu}{\rho} \nabla^2 \vec{v}_f + \rho_f g \tag{2}$$

$$\frac{\partial (\rho_f c_{p,f} T_f)}{\partial t} + \nabla \cdot (\rho_f c_{p,f} T_f \vec{v}_f) = \nabla \cdot (k_f \nabla T_f) + \dot{Q}_r \tag{3}$$

$$\rho_b c_{p,b} \frac{\partial T_b}{\partial t} = \frac{k_{b,r}}{r} \frac{\partial}{\partial r} \left(r \frac{\partial T_b}{\partial r} \right) + \frac{k_{b,\theta}}{r^2} \frac{\partial^2 T_b}{\partial \theta^2} + k_{b,z} \frac{\partial^2 T_b}{\partial z^2} + \dot{Q}_{gen} \tag{4}$$

At the fluid–solid interface, conductive heat transfer was coupled with convective and radiative exchange, modeled as:

$$-\hat{\mathbf{n}} \cdot \mathbf{q} = h\left(T_\infty - T_f\right) + \varepsilon\sigma\left(T_\infty^{\,4} - T_f^{\,4}\right) \tag{5}$$

where h is the convective heat transfer coefficient, ε is emissivity, and σ is the Stefan–Boltzmann constant.

Heat generation within a LIB cell was divided into two stages:

Stage I – Operational heat: arises from thermodynamic and ohmic losses during charge/discharge cycles. It is expressed as:

$$\dot{Q}_{TO} = I\left(T \frac{dU_{OC}}{dT}\right) + I^2 R \tag{6}$$

where the internal resistance (R) and entropic heat coefficient (dU_{OC}/dT) depend on the cell temperature and state of charge (SOC) [3].

Stage II – Abuse reaction heat: initiated when cell temperature exceeds ~60 °C, leading to a cascade of decomposition and electrochemical reactions. The total abuse heat is represented as:

$$\dot{Q}_{TR} = \dot{Q}_{SEI} + \dot{Q}_{an} + \dot{Q}_{ele} + \dot{Q}_{ca} + \dot{Q}_{ec} \tag{7}$$

where terms correspond to SEI decomposition, anode–electrolyte reactions, cathode–electrolyte reactions, electrolyte decomposition, and secondary electrochemical reactions.

Each reaction follows an Arrhenius-type rate law, dependent on activation energy, frequency factor, and reactant concentration as below:

$$\dot{Q}_i(T, c_i) = H_i W_i A_i c_i \exp\left(-\frac{E_{a,i}}{RT}\right) \quad (8)$$

$$\frac{dc_i}{dt} = -A_i c_i \exp\left(-\frac{E_{a,i}}{RT}\right) \quad (9)$$

Heat production from the electrochemical reactions [9]:

$$\dot{Q}_{ec}(T, SOC) = -\eta \cdot U_{cell} \cdot 3600 \cdot C_{cell} \cdot SOC \cdot A_{ec} \cdot \exp\left(-\frac{E_{a,ec}}{RT}\right) \quad (10)$$

$$\frac{d\,SOC}{dt} = -\frac{I}{3600 \cdot C_{cell}} \quad (11)$$

An efficiency factor of $\eta = 0.28$ is used [10]. Here, C_{cell} denotes the cell capacity. The kinetic parameters for the reactions mentioned above are presented in Table 1.

The SIMPLE algorithm was employed for pressure–velocity coupling, while the Realizable k–ε turbulence model described airflow characteristics. Second-order upwind discretization was used for momentum, energy, and turbulence equations. Enhanced wall treatment was applied to improve accuracy near cell surfaces.

Table 1. Kinetic parameters and enthalpies of thermal abuse model [9, 11].

	SEI	**anode**	**cathode**	**electrolyte**	**SOC**
Frequency factor, A [s^{-1}]	1.667×10^{15}	2.5×10^{13}	6.667×10^{13}	5.14×10^{25}	2.87×10^{4}
Activation energy, E_a [J/mol]	1.3508×10^{5}	1.3508×10^{5}	1.396×10^{5}	2.74×10^{5}	1.247×10^{5}
Specific heat release, H [J/kg]	2.57×10^{5}	1.714×10^{6}	3.14×10^{5}	1.55×10^{5}	–
Specific content, W [kg/m^3]	610.4	610.4	1438	406.9	–
Initial value [–]	0.15	0.75	0.04	1.00	

3 Results and discussion

Before applying the model to large-scale modules, a preliminary case of a single cell undergoing TR was simulated to evaluate accuracy. A grid independence study was first conducted to balance computational cost with accuracy in capturing flow and thermal responses. A mesh with 529,008 tetrahedral elements was determined to be optimal and used for all subsequent simulations.

Model validation was performed against experimental data of [12, 13], in which commercial 18650 cells were heated in an oven. As shown in Fig. 2, simulated temperature profiles followed the same trends as experimental results: a gradual increase during heating, a sharp rise once the runaway threshold was reached, and a final decline toward the oven temperature after failure. The model successfully reproduced the three characteristic points of thermal abuse: (i) the self-heating temperature, defined as the inflection point where the second derivative of temperature changes sign; (ii) the onset temperature, identified when the heating rate exceeds 2 °C/min; and (iii) the maximum temperature reached during TR. The simulated peak temperatures deviated from experimental values by less than 5%, confirming the suitability of the model for capturing TR dynamics.

The sequence of side reactions during thermal abuse was further analyzed in terms of concentration variations, heat flows, and cell temperature (Fig. 3). SEI decomposition initiated at ~88 °C after 32 minutes, releasing the first wave of heat. If adequately dissipated, this stage does not lead to TR; however, insufficient cooling triggers subsequent exothermic reactions. The anode–electrolyte reaction followed at 134 °C (53 minutes), producing self-heating that rapidly escalated the temperature. The cathode began decomposing at 151 °C,

and together with anode reactions, drove the system into full TR at ~153 °C. Electrolyte decomposition and internal short circuiting occurred beyond 200 °C, leading to abrupt temperature spikes and complete consumption of reactive materials.

These results highlight the critical role of early-stage heat dissipation. Preventing or delaying the transition from SEI decomposition to self-heating can suppress TR initiation even under abusive conditions. This underlines the necessity of a robust battery thermal management system (BTMS) capable of removing localized heat before exothermic cascades occur.

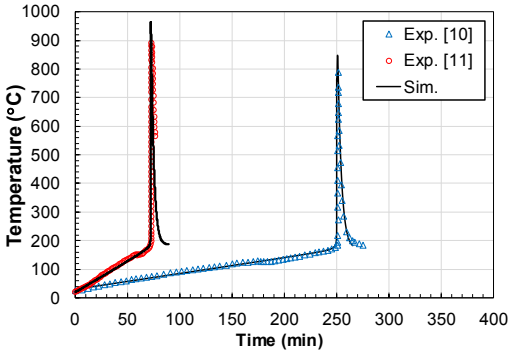

Fig. 2. Temperature evolution of LIBs during the TR process comparing with experimental data.

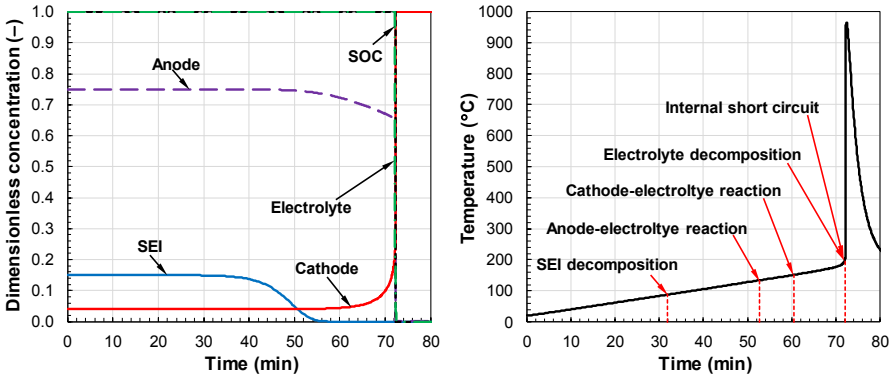

Fig. 3. Simulated evolutions of dimensionless concentrations, and cell temperature.

The validated model was next applied to a Tesla Model S module under pressurized air cooling. Discharge currents were based on realistic driving cycles [14], with average and peak values of 0.25 A and 2.7 A (0.2C and 0.8C rates). Simulation results (Fig. 4) revealed that increasing the Reynolds number (Re) of airflow significantly reduced both the maximum cell temperature and temperature non-uniformity within the module. At 0.2C discharge, thermal conditions remained within safe limits [8] when Re exceeded 8,800 and 21,000, corresponding to convective coefficients of ~26 W/m²·K and ~65 W/m²·K.

Although severe conditions at 0.8C discharge temporarily pushed the system beyond uniformity constraints, these high loads occur only intermittently during real driving. Pressurized air cooling with Re > 21,000 was shown to maintain safe operation without long-term heat accumulation, demonstrating its practicality for large-scale modules.

The thermal response of cells adjacent to the failed cell under varying airflow rates is shown in Fig. 5. Upstream failures (FB5, FB6) produced lower neighboring cell temperatures compared to downstream (FB2) or core failures (FB3, FB4), due to the cooling effect of fresh incoming air. The highest cell temperatures consistently occurred downstream of the failed

cell, reflecting dominant convective transport of heat. In contrast, FB1 failures (rear-edge) produced the lowest surrounding temperatures since no downstream cells were present.

Increasing Re effectively suppressed propagation in all scenarios. At Re > 48,000, TR could be prevented entirely in most cases, except when failures occurred in the first-row cells (FB5, FB6). This exception arises because cells in subsequent rows benefit from higher turbulence and thinner boundary layers, which enhance convective cooling. At sufficiently high airflow rates, however, even first-row failures can be suppressed.

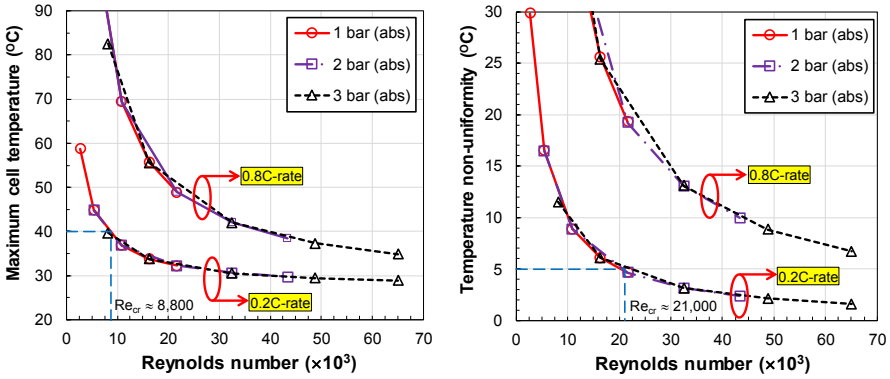

Fig. 4. Effect of Reynolds number on maximum temperature, and temperature non-uniformity.

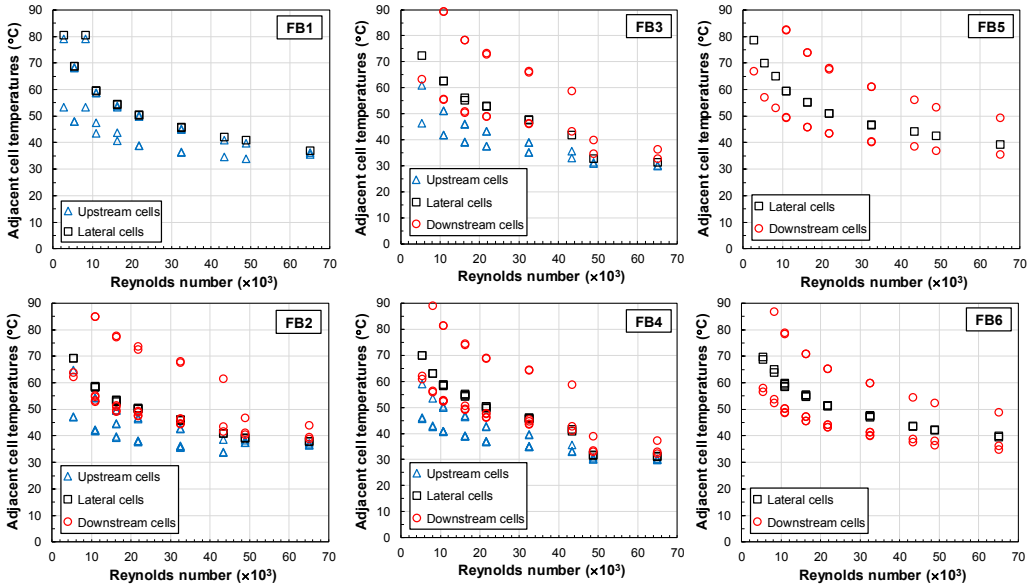

Fig. 5. Variation of temperature in cells surrounding the failed cell with the Reynolds numbers.

4 Conclusion

This study develops a three-dimensional thermal model of a pressurized air cooling system to assess TRP in large-scale LIB packs. Using a Tesla Model S module with 444 cells (74P6S) as a case study, the effects of heat dissipation rate and failure location were examined under over-discharge conditions. The key findings are as follows:

- The proposed thermal abuse model closely matches experimental data, with <5% error in maximum temperature prediction.
- Early SEI decomposition is the critical trigger for runaway; rapid cooling at this stage is essential for suppression.
- Pressurized air cooling significantly improves thermal management, maintaining safe operating conditions at Re > 21,000.
- Failure propagation is strongly influenced by initiation site, with downstream cells most vulnerable.
- Increasing airflow turbulence enhances cooling effectiveness, and Re > 48,000 can prevent runaway propagation across the module.

Overall, these results confirm that pressurized air cooling is a viable BTMS strategy for mitigating TRP in large-format LIB modules, provided airflow is sufficiently intense and uniformly distributed. Future work should focus on evaluating long-term aging effects, cell-to-cell thermal and electrochemical non-uniformity, and system performance under realistic operating conditions to ensure reliable and scalable practical implementation.

This research budget was allocated by National Science, Research and Innovation Fund (NSRF), and King Mongkut's University of Technology North Bangkok (Project no. KMUTNB-FF-70-B-33); and Thailand Science Research and Innovation Fundamental Fund fiscal year 2027.

References

1. A.W. Golubkov, D. Fuchs, J. Wagner, H. Wiltsche, C. Stangl, G. Fauler, G. Voitic, A. Thaler, V. Hacker, Thermal-runaway experiments on consumer Li-ion batteries with metal-oxide and olivin-type cathodes. RSC Adv. **4**, 3633-3642 (2014).
2. S. Ubaldi, P. Russo, Comparison between 18650 Lithium-ion cells of different composition subjected to thermal abuse. Chem. Eng. Trans., **104**, 49-54 (2023).
3. I. Dhuchakallaya, P. Saechan, Enhancing the cooling efficiency of the air cooling system for electric vehicle battery modules through liquid spray integration. J. Energy Storage. **72**, 108751 (2023).
4. P. Saechan, I. Dhuchakallaya, F.A.Z.M. Saat, Thermal Performance Improvement of Forced-Air Cooling System Combined with Liquid Spray for Densely Packed Batteries of Electric Vehicle. Eng. Sci., **24,** 886 (2023).
5. I. Dhuchakallaya, P. Saechan, Numerical study of a pressurized gas cooling system to suppress thermal runaway propagation in high-energy-density lithium-ion battery packs. J. Energy Storage, **101,** 113916 (2024).
6. C. Qi, Y. Zhu, F. Gao, K. Yang, Q. Jiao, Mathematical model for thermal behavior of lithium ion battery pack under overcharge. Int. J. Heat Mass Transf. **124,** 552-563 (2018).
7. X. Feng, X. He, M. Ouyang, L. Lu, P. Wu, C. Kulp, S. Prasser, Thermal runaway propagation model for designing a safer battery pack with 25Ah LiNixCoyMnzO2 large format lithium ion battery. App. Energy. **154,** 74-91 (2015).
8. P. Saechan, I. Dhuchakallaya, Numerical investigation of air cooling system for a densely packed battery to enhance the cooling performance through cell arrangement strategy. Int. J. Energy Res. **46**(14), 20670-20684 (2022).
9. T.T.D. Nguyen, Understanding and modelling the thermal runaway of Li-ion batteries. Ph.D. Thesis, Université de Picardie Jules Verne, France, 2021.

10. P.T. Coman, E.C. Darcy, C.T. Veje, R.E. White, Modelling Li-ion cell thermal runaway triggered by an internal short circuit device using an efficiency factor and arrhenius formulations. J. Electrochem. Soc. **164**(4), A587-A593 (2017).
11. G.-H. Kim, A. Pesaran, R. Spotnitz, A three-dimensional thermal abuse model for lithium-ion cells. J. Power Sources. **170**(2), 476-489 (2007).
12. A. Königseder, Investigation of the thermal runaway in Lithium ion batteries. Master Thesis, Graz University of Technology, Austria, 2017.
13. A.W. Golubkov, S. Scheikl, R. Planteu, G. Voitic, H. Wiltsche, C. Stangl, G. Fauler, A. Thaler, V. Hacker, Thermal runaway of commercial 18650 Li-ion batteries with LFP and NCA cathodes – impact of state of charge and overcharge. RSC Adv. **5**(70), 57171-57186 (2015).
14. M. Ragone, V. Yurkiv, A. Ramasubramanian, B. Kashir, F. Mashayek, Data driven estimation of electric vehicle battery state-of-charge informed by automotive simulations and multi-physics modeling. J. Power Sources. **483**, 229108 (2021).